

LFSamba: Marry SAM with Mamba for Light Field Salient Object Detection

Zhengyi Liu*, Longzhen Wang, Xianyong Fang, Zhengzheng Tu, Linbo Wang

Abstract—A light field camera can reconstruct 3D scenes using captured multi-focus images that contain rich spatial geometric information, enhancing applications in stereoscopic photography, virtual reality, and robotic vision. In this work, a state-of-the-art salient object detection model for multi-focus light field images, called LFSamba, is introduced to emphasize four main insights: (a) Efficient feature extraction, where SAM is used to extract modality-aware discriminative features; (b) Inter-slice relation modeling, leveraging Mamba to capture long-range dependencies across multiple focal slices, thus extracting implicit depth cues; (c) Inter-modal relation modeling, utilizing Mamba to integrate all-focus and multi-focus images, enabling mutual enhancement; (d) Weakly supervised learning capability, developing a scribble annotation dataset from an existing pixel-level mask dataset, establishing the first scribble-supervised baseline for light field salient object detection. <https://github.com/liuzywen/LFScribble>

Index Terms—SAM, Mamba, multi-focus, light field, salient object detection

I. INTRODUCTION

Light field (LF) cameras [1] play an important role in stereoscopic photography, virtual reality, and robotic vision applications, because they can reconstruct 3D scenes via multi-view and multi-focus images. Multi-view images [2], [3] reflect the panoramic views of objects, effectively addressing the occlusion problem, while multi-focus images [4] perceive the spatial context of objects, benefiting the partition of foreground objects and background. Fig 1 presents examples of multi-focus images, which typically consist of some focal slices focused at different depth levels and an all-focus image synthesized from all focal slices via photo-montage technique. Each focal slice asynchronously focuses on different depth positions and blur the others, while the all-focus image simultaneously depicts the full scene appearance and ignore the depth of field of objects.

Salient object detection (SOD) in multi-focus images can extract attractive objects for the observers based on both all focal slices and all-focus images. Compared with the current predominant method which finetunes Segment Anything Model (SAM) [5] using adapters [6] exclusively on all-focus images, our method locates the correct salient objects by perceiving the depth information embedded in multi-focus images, as shown in Fig 1. Three key perspectives which benefit SOD task for multi-focus LF images will be elaborated.

Zhengyi Liu, Longzhen Wang, Xianyong Fang, Zhengzheng Tu, and Linbo Wang are with the School of Computer Science and Technology, Anhui University, Hefei, China (e-mail: liuzywen@ahu.edu.cn, 1774537072@qq.com, fangxianyong@ahu.edu.cn, zhengzhengahu@163.com, wanglb@ahu.edu.cn). Zhengyi Liu is the corresponding author. This work is supported by National Natural Science Foundation of China under Grant 62376005.

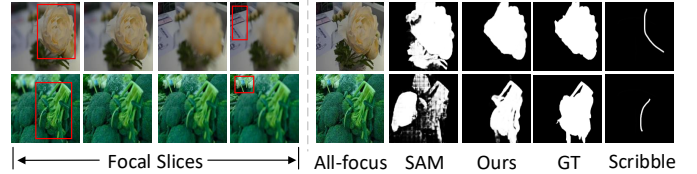


Fig. 1. Examples of multi-focus light field images. Each example consists of a set of focal slices and an all-focus image. Red boxes indicate the focused region. Compared with “SAM” finetuned exclusively on the all-focus image, “Ours” finetuned on multi-focus images are closer to the pixel-level mask annotation “GT”. “Scribble” refers to the sparse annotation.

Feature extraction ability: Detecting salient objects that attract observers requires a highly effective feature extractor. In the past few years, transformer encoders have outperforms convolutional ones [7]. Based on long range dependency of transformer framework and massive amount of training samples, SAM has been widely used to encode features, showing the discriminative advantage. However, in LF SOD task, it is necessary to encode multiple focal slices along with an all-focus image. To both mitigate the computation cost and enhance feature discrimination, a frozen SAM encoder with a group of fine-tuned adapters is used to encode focal slice features and all-focus features.

Fusion ability: Fusion in light field includes fusion among different focal slices and fusion between focal slices and all-focus images. The former is the sequence fusion of the images with the same modality, while the later is multi-modal fusion. Because Mamba can model long-range dependencies in long sequence data [8], it is adopted to process the sequence of focal slices, extracting implicit spatial structure information from the scenes. Furthermore, an inter-modal Mamba is designed to achieve multi-modal fusion, highlighting commonalities and suppressing redundancies.

Weakly supervised learning ability: Annotation is important for deep learning model to learn latent mapping from input to output. Existing methods trained LF SOD models via dense annotation with high labor costs. To eliminate the labelling overhead, a scribble annotation dataset and a weak supervised learning method is constructed and exploited, respectively. The last column of Fig 1 gives annotation examples which use sparse scribbles to indicate the foreground [9].

II. METHOD

A. Model pipeline

The proposed LFSamba is a two-stream encoder-decoder framework based on SAM. In the encoder part, a shared and frozen SAM encoder with the finetuned adapters is used to

extract focal slice features and all-focus features, respectively. An Inter-Slice Mamba is proposed to integrate all focal slice features in different depth levels. Furthermore, an inter-modal mamba is proposed to fuse focal slice features and all-focus features which are different in modality. Finally, the fused features are fed into SAM decoder to output the saliency map. The fully-supervised model is trained with the supervision of pixel-level ground truth, while the weakly-supervised model is trained with the supervision of our constructed scribble annotation. The whole architecture is shown in Fig. 2.

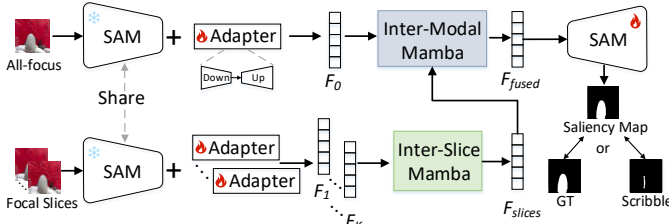


Fig. 2. The pipeline of LFSamba.

B. Feature extraction by large model SAM

Motivation. Recently the large model SAM has been proposed to achieve class-agnostic segmentation task. However, the zero-shot capability of SAM is not sufficiently robust to adapt to LF SOD task. Therefore, fine-tuning SAM using adapters offers an alternative approach for extracting features from light field images.

Design. Given an all-focus image I_r and its corresponding focal stack with K focal slices $\{I_{f_k}\}_{k=1}^K$, an SAM encoder with $K+1$ groups of finetuned adapters is used to generate all-focus features F_0 and focal slice features $\{F_k\}_{k=1}^K$.

$$F_0 = \mathcal{E}_{Adapter_0}(I_r) \quad (1)$$

$$F_k = \mathcal{E}_{Adapter_k}(I_{f_k}) (k = 1, \dots, K) \quad (2)$$

where $\mathcal{E}_{Adapter_k} (k = 0, \dots, K)$ is a frozen SAM encoder with the k -th group of adapter, subscript $k = 0$ is the all-focus indicator, while $k = 1, \dots, K$ are focal slice indicators. Each group of adapters includes a position adapter and some feature adapters. The position adapter is a max pooling operation followed a convolution operation with a kernel size of 3×3 conducted on position embedding. It is responsible for adapting the model to the input with a smaller size (256×256) rather than the original size (1024×1024) used in vanilla SAM, aiming to reduce the computation cost. The feature adapter is a bottleneck structure, which consists of a down-projection layer, a ReLU layer, and an up-projection layer, in parallel with multi-layer perceptron (MLP) layer of transformer block in vanilla SAM encoder. It is in charge of extracting modality-aware all-focus feature and focal slice features.

C. Feature integration within slices via inter-slice mamba

Motivation. The multi-focus image includes a set of focal slices which show the similar appearance and different focused region. To integrate all the focal slices, many technologies have been applied. MEANet [10] conducted concatenation operation in input level, ignoring the correlation among slices.

SA-Net [11], DLGLRG [12], and LFTransNet [13] used 3D convolution, graph network, and transformer, respectively. However, these methods consumed a large computational overhead. LFNet [14], MoLF [15], ERNet [16], and NoiseLF [17] employed ConvLSTM [18] to learn spatial structures recurrently, but the local convolutional nature made it less effective at capturing long-range dependencies among focal slices.

Recently, Mamba [8], derived from State Space Models (SSMs) [19], has advanced deep learning models due to their capability of modeling long sequences to achieve global receptive fields with linear complexity. Vision Mamba [20] integrated SSM with bidirectional scanning, making each patch related to another. Meanwhile, VMamba [21] extended scanning in four directions in the proposed 2D Selective Scan (SS2D). To excavate latent information in the focal slices, SS2D is adopted to integrate all the focal slices.

Design. As shown in Fig 3 (a), the focal slice features are respectively fed into linear projection (Linear), depth-wise convolution (DWConv), and a SiLU activation layer.

$$P_k = \text{SiLU}(\text{DWConv}(\text{Linear}(F_k))) (k = 1, \dots, K) \quad (3)$$

Then, Focal SS2D (FSS2D) is designed to model the long-range dependency among all the focal slices.

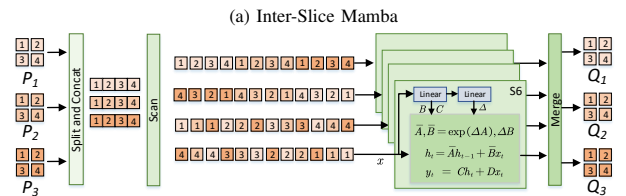
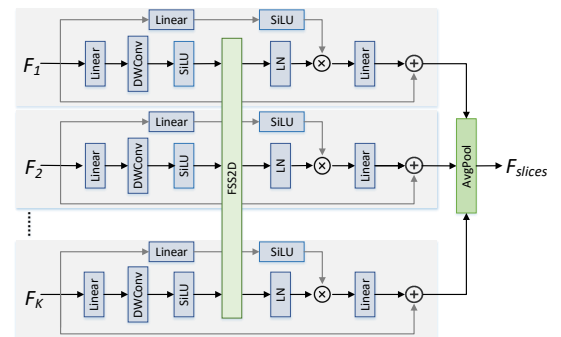
$$\{Q_1, \dots, Q_K\} = \text{FSS2D}(\{P_1, \dots, P_K\}) \quad (4)$$

Next, a layer normalization (LN), a multiplicative branch, and a residual connection are successively followed in each slice feature, where $k = 1, \dots, K$.

$$R_k = F_k + \text{Linear}(\text{LN}(Q_k) \times \text{SiLU}(\text{Linear}(F_k))) \quad (5)$$

Last, all the focal slice features are integrated via a concatenation and an averaged pooling operation.

$$F_{\text{slices}} = \text{AvgPool}(\text{Concat}(R_1, \dots, R_K)) \quad (6)$$



(b) FSS2D (Taking $K = 3$ as an example)

Fig. 3. Inter-Slice Mamba and its core component FSS2D.

Specifically, in FSS2D illustrated in Fig 3 (b), all the focal slice features $\{P_k\}_{k=1}^K$ are split into patches with the length L , and then concatenated in the second dimension to attain an integrated feature with the size of $K \times L$. Then, the integrated

feature is successively unfolded along four directions (row-wise and column-wise top-left to bottom-right, row-wise and column-wise bottom-right to top-left). Each patch sequence is fed into a separate S6 block [8] to extract multi-focal information along the different directions. Lastly, the four sequences are reversed to the original feature size. By FSS2D, intra-slice and inter-slice both perform forward and backward scanning, thereby each pixel is enhanced by integrating information from all other pixels in different positions in the same slice and the same position in different slices. The receptive fields of features are effectively enlarged to emphasize on the important information and suppress the redundancies in the focal slices.

D. Feature fusion between focal slices and all-focus via Inter-Modal Mamba

Motivation. The all-focus images emphasize on the overall appearance of the scene, while the focal slices focus on the regions with different depths and blur the other regions. The two-modal features have been shown to be complementary [13]. Mamba constructs intra-image global receptive field by introducing data-dependent parameters (B , C , Δ). In terms of two-modal features, the exchange of some parameters is beneficial for the mutual guidance, thereby proposing Slices-To-All SS2D and the reversed All-To-Slices SS2D.

Design. As shown in the middle stream of Fig 4 (a), the all-focus feature F_0 and the focal slice features F_{slices} are initially concatenated and convoluted to attain a basic fused feature P .

$$P = Conv(Concat(F_0, F_{slices})) \quad (7)$$

Then, the basic fused feature is successively fed into Linear, DWConv, SiLU, and an SS2D layer, followed by an LN and a Linear.

$$\bar{P} = Linear(LN(SS2D(SiLU(DWConv(Linear(P)))))) \quad (8)$$

Next, in terms of all-focus F_0 and focal slices features F_{slices} as shown in the top and bottom stream of Fig 4 (a), an slices-to-all (S2A) and a reversed all-to-slices (A2S) SS2D are applied to achieve the mutual guidance and complements.

$$x_0 = SiLU(DWConv(Linear(F_0))) \quad (9)$$

$$\bar{F}_0 = Linear(LN(S2A(x_0))) \quad (10)$$

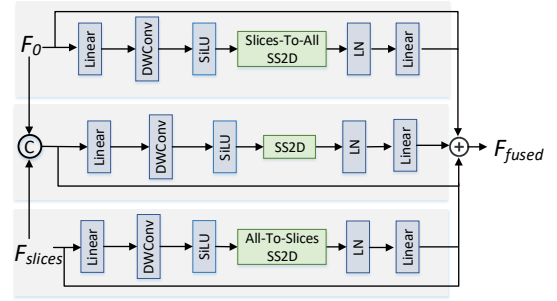
$$x_{slices} = SiLU(DWConv(Linear(F_{slices}))) \quad (11)$$

$$\bar{F}_{slices} = Linear(LN(A2S(x_{slices}))) \quad (12)$$

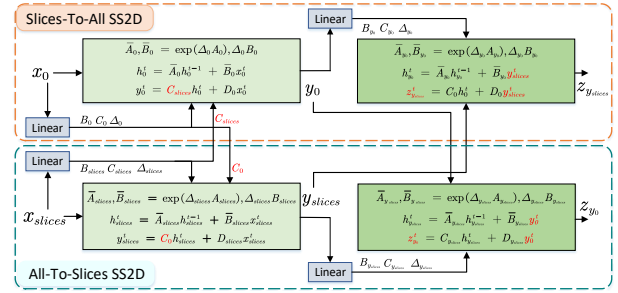
Last, three features are fused by addition operation after appending residual connections.

$$F_{fused} = \bar{F}_0 + F_0 + \bar{P} + P + \bar{F}_{slices} + F_{slices} \quad (13)$$

Specifically, in S2A and A2S SS2D, illustrated in Fig 3 (b), two-step SS2Ds are conducted. In the first step, the output matrixes C_{slices} and C_0 are exchanged to introduce the guidance of the other modality in the output matrices. In the second step, the output y_0 and y_{slices} of the first step are regarded as the input. To comprehensively interact with the information between the two modalities, y_{slices} and y_0 are exchanged, which essentially switches the input metric, output metric, and the state transition matrix between the two modalities so as to encourage a deeper integration.



(a) Inter-Modal Mamba



(b) Slices-To-All SS2D and All-To-Slices SS2D

Fig. 4. Inter-Modal Mamba and its core component Slices-To-All SS2D and All-To-Slices SS2D.

E. Decoding and supervision

The above fused feature is last fed into SAM decoder \mathcal{D} to generate the saliency map S .

$$S = \mathcal{D}(F_{fused}) \quad (14)$$

In fully supervised method, the weighted binary cross entropy loss and weighted IoU loss in [22] are adopted. In weakly supervised method, partial cross entropy loss, local saliency coherence loss, smoothness loss in [23] are employed.

III. EXPERIMENTS

A. Datasets

LF SOD dataset includes LFSD[24], HFUT-Lytro[25], and DUTLF-FS[26]. The training samples include 1,000 samples from DUTLF-FS and 100 samples from HFUT-Lytro, and the rest is used for testing. The scribble annotation is manually created by drawing both a foreground and a background scribble using the Image Labeler tool provided by MATLAB.

B. Comparison with State-of-the-art Methods

The comparison experiments of two different supervision settings are conducted on an NVIDIA RTX 4090 GPU. Experiment settings follow LFTransNet [13]. The top of Table I shows the quantitative comparisons with 15 fully-supervised methods. LFSamba outperforms the other fully supervised competitors with a large margin. It attributes to a good feature extractor which adopts SAM with finetuned adapters, an effective focal slice feature integration method which applied Inter-Slice Mamba, an optimal multi-modal fusion method which employs Inter-Modal Mamba. Moreover, the PR curves in Fig. 5 further confirm the strength of LFSamba, as its curve approaches the upper right corner.

TABLE I

Quantitative comparisons with **fully and weakly** supervised LF SOD methods on three LF SOD datasets. The best results are in bold.

Methods	Source	Supervision Type	LFSOD				HFUT-Lytro				DUTLF-FS			
			$S \uparrow$	$F_{\beta} \uparrow$	$E_{\xi} \uparrow$	MAE \downarrow	$S \uparrow$	$F_{\beta} \uparrow$	$E_{\xi} \uparrow$	MAE \downarrow	$S \uparrow$	$F_{\beta} \uparrow$	$E_{\xi} \uparrow$	MAE \downarrow
MoLF[15]	NeurIPS19	full	.830	.819	.886	.089	.742	.627	.785	.095	.887	.843	.923	.052
DLFS[27]	IJCAI19	full	.735	.713	.805	.149	.741	.616	.784	.097	.841	.801	.891	.076
LFNet[14]	TIP20	full	.806	.793	.870	.101	.781	.659	.808	.076	.882	.842	.914	.054
ERNet[16]	AAAI20	full	.835	.839	.887	.082	.778	.705	.831	.082	.900	.888	.942	.040
SA-Net[11]	BMVC21	full	.841	.845	.889	.074	.784	.736	.850	.078	.918	.920	.954	.032
DLGLRG[12]	ICCV21	full	.867	.861	.898	.069	.766	.709	.841	.071	.928	.923	.952	.031
PANet[28]	TCYB21	full	.849	.848	.893	.076	.795	.724	.851	.074	.908	.897	.940	.039
MEANet[10]	NEUCOM22	full	.851	.849	.888	.077	.796	.722	.850	.073	.931	.920	.951	.032
DGENet[29]	IVC23	full	.847	.839	.890	.075	.771	.692	.825	.084	.897	.881	.944	.040
TENet[30]	IVC23	full	.872	.862	.901	.063	.838	.791	.877	.059	.940	.940	.966	.023
GFRNet[31]	ICME23	full	.857	.859	.906	.065	.803	.756	.852	.072	.931	.941	.965	.026
LFTransNet[13]	TCSVT23	full	.905	.900	.925	.047	.838	.775	.869	.062	.941	.937	.962	.022
STSA[32]	TPAMI24	full	.871	.872	.910	.062	.834	.804	.880	.057	.928	.929	.964	.027
FES[33]	TMM24	full	.888	.883	.909	.052	.846	.800	.872	.062	.951	.954	.971	.018
LFSOD-Net[34]	TCSVT24	full	.889	.880	.911	.053	.835	.784	.871	.066	.943	.943	.963	.022
Ours	-	full	.914	.909	.929	.039	.874	.821	.893	.051	.957	.959	.973	.016
WSS[35]	CVPR17	category	.779	.771	.837	.140	.713	.602	.744	.122	.771	.743	.840	.126
MWS[36]	CVPR19	multiple	.809	.785	.834	.130	.723	.604	.732	.127	.829	.793	.875	.104
SCA[37]	CVPR20	scribble	.786	.782	.823	.107	.726	.633	.779	.098	.825	.814	.880	.075
SBB[38]	TIP21	box	.816	.816	.858	.097	.723	.628	.785	.099	.832	.819	.895	.076
SCWS[39]	AAAI21	scribble	.802	.794	.822	.099	.727	.668	.788	.098	.853	.844	.888	.063
WSLF [40]	TIP22	box	.831	.835	.880	.080	.727	.652	.794	.097	.889	.884	.937	.043
Ours	-	scribble	.883	.887	.902	.057	.849	.790	.879	.054	.918	.918	.948	.035

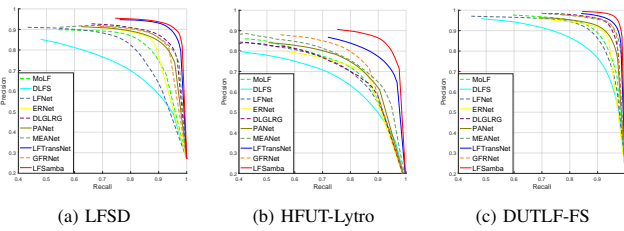


Fig. 5. The comparison of PR curves on three datasets.

The bottom of Table I shows the quantitative comparisons with 6 weakly supervised methods. Our method uses sparse scribble annotation. Compared with the other weakly supervised methods, our method maintains an outstanding level. The average reduction in MAE values across the three datasets reaches 31%.

C. Ablation studies

Table II shows the contributions of all the components. SAM endowed with adapters plays an important role in improving the performance. The evaluation metrics in the first row have outperformed most existing methods. Meanwhile, Inter-Slice Mamba and Inter-Modal Mamba work together to effectively pulls up the indicators, achieving state-of-the-art performance. Furthermore, to verify the roles of Mambas, the result using Concatenation, ConvLSTM, and Transformer are illustrated in the last three rows. The average reduction in MAE values across the three datasets reaches 14%, which validating the effect of Mamba. Table III compares the computation cost. ConvLSTM is a high-cost method, while Concatenation is the least expensive. Compared to the Transformer, Mamba exhibits lower time complexity. Fig 6 gives the feature map visualization. Compared F_{concat} , F_{lstm} , and F_{trans} with F_{slices} , the advantages of Inter-Slice Mamba in fusing focal slices are clearly evident from the object outlines. The complementary all-focus feature F_0 and focal slices feature F_{slices} are combined through Inter-Modal Mamba to create the optimal fused feature F_{fused} .

TABLE II

Ablation study about Adapter \heartsuit , Inter-Slice Mamba \clubsuit , and Inter-Modal Mamba \spadesuit based on Baseline \heartsuit . The last three rows show the results of integrating focal slices by Concatenation \square , ConvLSTM \triangle , and Transformer \diamond , respectively.

Variant	LFSOD				HFUT-Lytro				DUTLF-FS			
	$S \uparrow$	$F_{\beta} \uparrow$	$E_{\xi} \uparrow$	MAE \downarrow	$S \uparrow$	$F_{\beta} \uparrow$	$E_{\xi} \uparrow$	MAE \downarrow	$S \uparrow$	$F_{\beta} \uparrow$	$E_{\xi} \uparrow$	MAE \downarrow
\heartsuit	.896	.892	.923	.050	.817	.760	.858	.070	.940	.942	.966	.023
$\heartsuit\clubsuit$.903	.898	.927	.044	.859	.812	.888	.059	.948	.945	.968	.019
$\heartsuit\spadesuit$.911	.905	.924	.042	.867	.807	.879	.055	.956	.954	.968	.017
$\heartsuit\clubsuit\spadesuit$.904	.904	.920	.045	.864	.799	.883	.053	.954	.956	.971	.018
$\heartsuit\clubsuit\spadesuit$.914	.909	.929	.039	.874	.821	.893	.051	.957	.959	.973	.016
$\heartsuit\square$.901	.889	.925	.045	.857	.811	.883	.057	.953	.951	.968	.019
$\heartsuit\triangle$.903	.896	.924	.046	.860	.800	.880	.058	.953	.950	.965	.019
$\heartsuit\diamond$.899	.895	.921	.045	.867	.807	.884	.054	.949	.940	.967	.020

TABLE III

Computation cost comparison among Concatenation, ConvLSTM, and Transformer, and our Mamba.

Variant	Concatenation	ConvLSTM	Transformer	Our Mamba
Params (M) \downarrow	328	387	380	359
FLOPs (G) \downarrow	305	377	369	324
FPS (Hz) \uparrow	3.1	2.8	3.0	3.1

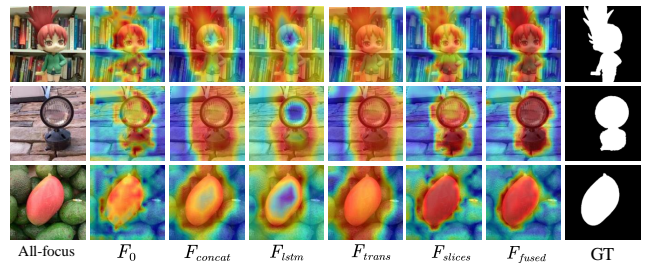


Fig. 6. Feature Maps Visualization.

IV. CONCLUSIONS

A light field salient object detection model LFSamba is proposed. It introduces SAM to extract the discriminative features, employs Mamba to model long-range dependency among focal slices and interact all-focus and multi-focal features, and last provides a scribble supervised baseline. LFSamba achieves a significant improvement in performance. The model requires a significant computational cost, highlighting the need for a lightweight version in the future.

REFERENCES

- [1] D. He, C. Liu, L. Wu, and J. Qiu, "Light field surface feature and spherical descriptor in the surface scale space," *IEEE Signal Processing Letters*, pp. 803–807, 2023.
- [2] B. Yuan, Y. Jiang, K. Fu, and Q. Zhao, "Parallax-aware network for light field salient object detection," *IEEE Signal Processing Letters*, pp. 810–814, 2024.
- [3] S. Zhang and E. Y. Lam, "Light field image restoration via latent diffusion and multi-view attention," *IEEE Signal Processing Letters*, pp. 1094–1098, 2024.
- [4] A. Wang, "Three-stream cross-modal feature aggregation network for light field salient object detection," *IEEE Signal Processing Letters*, vol. 28, pp. 46–50, 2020.
- [5] A. Kirillov, E. Mintun, N. Ravi, H. Mao, C. Rolland, L. Gustafson, T. Xiao, S. Whitehead, A. C. Berg, W.-Y. Lo, P. Dollar, and R. Girshick, "Segment anything," in *Proceedings of the IEEE International Conference on Computer Vision*, 2023, pp. 4015–4026.
- [6] S. Chen, C. Ge, Z. Tong, J. Wang, Y. Song, J. Wang, and P. Luo, "AdaptFormer: Adapting vision transformers for scalable visual recognition," *Advances in Neural Information Processing Systems*, vol. 35, pp. 16 664–16 678, 2022.
- [7] A. Dosovitskiy, "An image is worth 16x16 words: Transformers for image recognition at scale," in *International Conference on Learning Representations*, 2021, pp. 1–22.
- [8] A. Gu and T. Dao, "Mamba: Linear-time sequence modeling with selective state spaces," in *Conference on Language Modeling*, 2024, pp. 1–36.
- [9] W. Li, X. Xiong, S. Li, and F. Fan, "Hybridvps: Hybrid-supervised video polyp segmentation under low-cost labels," *IEEE Signal Processing Letters*, pp. 111–115, 2023.
- [10] Y. Jiang, W. Zhang, K. Fu, and Q. Zhao, "MEANet: Multi-modal edge-aware network for light field salient object detection," *Neurocomputing*, vol. 491, pp. 78–90, 2022.
- [11] Y. Zhang, G. Chen, Q. Chen, Y. Sun, Y. Xia, O. Deforges, W. Hamidouche, and L. Zhang, "Learning synergistic attention for light field salient object detection," in *Proceedings of British Machine Vision Conference*, 2021, pp. 1–14.
- [12] N. Liu, W. Zhao, D. Zhang, J. Han, and L. Shao, "Light field saliency detection with dual local graph learning and reciprocative guidance," in *Proceedings of the IEEE/CVF International Conference on Computer Vision*, 2021, pp. 4712–4721.
- [13] Z. Liu, Q. He, L. Wang, X. Fang, and B. Tang, "LFTransNet: Light field salient object detection via a learnable weight descriptor," *IEEE Transactions on Circuits and Systems for Video Technology*, vol. 33, no. 12, pp. 7764–7773, 2023.
- [14] M. Zhang, W. Ji, Y. Piao, J. Li, Y. Zhang, S. Xu, and H. Lu, "LFNet: Light field fusion network for salient object detection," *IEEE Transactions on Image Processing*, vol. 29, pp. 6276–6287, 2020.
- [15] M. Zhang, J. Li, W. Ji, Y. Piao, and H. Lu, "Memory-oriented decoder for light field salient object detection," in *Proceedings of the 33rd International Conference on Neural Information Processing Systems*, 2019, pp. 898–908.
- [16] Y. Piao, Z. Rong, M. Zhang, and H. Lu, "Exploit and replace: An asymmetrical two-stream architecture for versatile light field saliency detection," in *Proceedings of the AAAI Conference on Artificial Intelligence*, 2020, pp. 11 865–11 873.
- [17] M. Feng, K. Liu, L. Zhang, H. Yu, Y. Wang, and A. Mian, "Learning from pixel-level noisy label: A new perspective for light field saliency detection," in *Proceedings of the IEEE/CVF Conference on Computer Vision and Pattern Recognition*, 2022, pp. 1756–1766.
- [18] X. Shi, Z. Chen, H. Wang, D.-Y. Yeung, W.-k. Wong, and W.-c. Woo, "Convolutional LSTM Network: A Machine Learning Approach for Precipitation Nowcasting," in *Proceedings of the 28th International Conference on Neural Information Processing Systems-Volume 1*, 2015, pp. 802–810.
- [19] A. Gu, K. Goel, and C. Re, "Efficiently modeling long sequences with structured state spaces," in *International Conference on Learning Representations*, 2022, pp. 1–27.
- [20] L. Zhu, B. Liao, Q. Zhang, X. Wang, W. Liu, and X. Wang, "Vision mamba: Efficient visual representation learning with bidirectional state space model," in *International Conference on Machine Learning*, 2024, pp. 1–14.
- [21] Y. Liu, Y. Tian, Y. Zhao, H. Yu, L. Xie, Y. Wang, Q. Ye, J. Jiao, and Y. Liu, "VMamba: Visual state space model," in *The Thirty-eighth Annual Conference on Neural Information Processing Systems*, 2024, pp. 1–33.
- [22] J. Wei, S. Wang, and Q. Huang, "F³Net: Fusion, feedback and focus for salient object detection," in *Proceedings of the AAAI Conference on Artificial Intelligence*, 2020, pp. 12 321–12 328.
- [23] Z. Liu, X. Huang, G. Zhang, X. Fang, L. Wang, and B. Tang, "Scribble-supervised RGB-T salient object detection," in *IEEE International Conference on Multimedia and Expo (ICME)*. IEEE, 2023, pp. 2369–2374.
- [24] N. Li, J. Ye, Y. Ji, H. Ling, and J. Yu, "Saliency detection on light field," in *Proceedings of the IEEE Conference on Computer Vision and Pattern Recognition*, 2014, pp. 2806–2813.
- [25] J. Zhang, M. Wang, L. Lin, X. Yang, J. Gao, and Y. Rui, "Saliency detection on light field: A multi-cue approach," *ACM Transactions on Multimedia Computing, Communications, and Applications (TOMM)*, vol. 13, no. 3, pp. 1–22, 2017.
- [26] T. Wang, Y. Piao, X. Li, L. Zhang, and H. Lu, "Deep learning for light field saliency detection," in *Proceedings of the IEEE/CVF International Conference on Computer Vision*, 2019, pp. 8838–8848.
- [27] Y. Piao, Z. Rong, M. Zhang, X. Li, and H. Lu, "Deep light-field-driven saliency detection from a single view," in *Proceedings of the Twenty-Eighth International Joint Conference on Artificial Intelligence*, 2019, pp. 904–911.
- [28] Y. Piao, Y. Jiang, M. Zhang, J. Wang, and H. Lu, "PANet: Patch-aware network for light field salient object detection," *IEEE Transactions on Cybernetics*, vol. 53, no. 1, pp. 379–391, 2021.
- [29] Y. Liang, G. Qin, M. Sun, J. Qin, J. Yan, and Z. Zhang, "Dual guidance enhanced network for light field salient object detection," *Image and Vision Computing*, vol. 118, pp. 1–13, 2022.
- [30] X. Wang, S. Chen, G. Wei, and J. Liu, "TENet: Accurate light-field salient object detection with a transformer embedding network," *Image and Vision Computing*, vol. 129, pp. 1–12, 2023.
- [31] B. Yuan, Y. Jiang, K. Fu, and Q. Zhao, "Guided focal stack refinement network for light field salient object detection," in *2023 IEEE International Conference on Multimedia and Expo (ICME)*. IEEE, 2023, pp. 2387–2392.
- [32] W. Gao, S. Fan, G. Li, and W. Lin, "A thorough benchmark and a new model for light field saliency detection," *IEEE Transactions on Pattern Analysis and Machine Intelligence*, pp. 8003–8019, 2023.
- [33] G. Chen, H. Fu, T. Zhou, G. Xiao, K. Fu, Y. Xia, and Y. Zhang, "Fusion-embedding siamese network for light field salient object detection," *IEEE Transactions on Multimedia*, pp. 984–994, 2024.
- [34] X. Zheng, Z. Li, D. Liu, X. Zhou, and C. Shan, "Spatial attention-guided light field salient object detection network with implicit neural representation," *IEEE Transactions on Circuits and Systems for Video Technology*, pp. 1–14, 2024.
- [35] L. Wang, H. Lu, Y. Wang, M. Feng, D. Wang, B. Yin, and X. Ruan, "Learning to detect salient objects with image-level supervision," in *Proceedings of the IEEE Conference on Computer Vision and Pattern Recognition*, 2017, pp. 136–145.
- [36] Y. Zeng, Y. Zhuge, H. Lu, L. Zhang, M. Qian, and Y. Yu, "Multi-source weak supervision for saliency detection," in *Proceedings of the IEEE/CVF Conference on Computer Vision and Pattern Recognition*, 2019, pp. 6074–6083.
- [37] J. Zhang, X. Yu, A. Li, P. Song, B. Liu, and Y. Dai, "Weakly-supervised salient object detection via scribble annotations," in *Proceedings of the IEEE/CVF Conference on Computer Vision and Pattern Recognition*, 2020, pp. 12 546–12 555.
- [38] Y. Liu, P. Wang, Y. Cao, Z. Liang, and R. W. Lau, "Weakly-supervised salient object detection with saliency bounding boxes," *IEEE Transactions on Image Processing*, vol. 30, pp. 4423–4435, 2021.
- [39] S. Yu, B. Zhang, J. Xiao, and E. G. Lim, "Structure-consistent weakly supervised salient object detection with local saliency coherence," in *Proceedings of the AAAI Conference on Artificial Intelligence*, 2021, pp. 3234–3242.
- [40] Z. Liang, P. Wang, K. Xu, P. Zhang, and R. W. Lau, "Weakly-supervised salient object detection on light fields," *IEEE Transactions on Image Processing*, vol. 31, pp. 6295–6305, 2022.